So $t_{\mu\nu}$ can be calculated using the fast Fourier transform, which involves $O(N \log_2 N)$ operations.

The vectors $\partial C/\partial f_{ijm}$ and $\mathbf{e}^3$ can be calculated in an analogous way. In total, six Fourier transforms are need in each cycle:

(i) one Fourier transform for the determination of F_{hkl} from the current EDD;

(ii) one Fourier transform for the determination of the vector $\partial C/\partial f_{ijm}$;

(iii) one Fourier transform for the determination of the vector $\mathbf{e}^3$;

(iv) three Fourier transforms for the determination of $t_{\mu\nu}$.

References

BAERT, F., COPPENS, P., STEVENS, E. D. & DEVOS, L. (1982). *Acta Cryst.* A**38**, 143–151.

BRUNING, H. & FEIL, D. (1992). *Acta Cryst.* A**48**, 865–872.

CRAVEN, B. M., WEBER, H. P. & HE, X. (1987). Technical Report TR-87-2. Department of Crystallography, Univ. of Pittsburgh, PA 15260, USA.

ERIKSSON, A. & HERMANSSON, K. (1983). *Acta Cryst.* B**39**, 703–711.

HANSEN, N. K. & & COPPENS, P. (1978). *Acta Cryst.* A**34**, 909–921.

HIRSHFELD, F. L. (1971). *Acta Cryst.* B**27**, 769–781.

HIRSHFELD, F. L. (1977). *Isr. J. Chem.* **16**, 226–229.

JAUCH, W. & PALMER, A. (1993). *Acta Cryst.* A**49**, 590–591.

JAYNES, E. T. (1983). (Collected works.) In *Papers on Probability, Statistics and Statistical Physics*, edited by R. D. ROSENKRANTZ. Dordrecht: Reidel.

LECOMTE, C. (1991). In *The Application of Charge Density Research to Chemistry and Drug Design*, edited by G. A. JEFFREY & J. F. PINIELLA. New York: Plenum.

SAKA, T. & KATO, N. (1986). *Acta Cryst.* A**42**, 469–478.

SAKATA, M. & SATO, M. (1990). *Acta Cryst.* A**46**, 263–270.

SKILLING J. & BRYAN, R. K. (1984). *Mon. Not. R. Astron. Soc.* **211**, 111–124.

Acta Cryst. (1994). A**50**, 391–402

Solution Scattering from Biopolymers: Advanced Contrast-Variation Data Analysis

BY D. I. SVERGUN*

European Molecular Biology Laboratory, Hamburg Outstation, Notkestrasse 85, *D*-22603 *Hamburg, Germany*

(*Received* 30 *September* 1993; *accepted* 1 *December* 1993)

Abstract

New approaches to the interpretation of contrast-variation data from monodisperse systems using spherical harmonics are presented. A general method is given for evaluating the particle shape and internal structure and expressions for the scattering from the density fluctuations inside a particle with a known shape are derived. Further, the scattering from two-component particles is analyzed in terms of the positions and/or shapes of the components and the information content of the contrast-variation data is discussed. The methods can be used for advanced low-resolution structure analysis of various types of biopolymers in solution.

Introduction

Small-angle scattering (SAS) is one of the most effective methods of investigating the superatomic structure of native biopolymers and their complexes in solution (Feigin & Svergun, 1987). The SAS intensity $I(s)$ of a dilute monodisperse solution of biopolymers is proportional to the scattering from a single particle averaged over all orientations [here s denotes the modulus of the scattering vector $\mathbf{s}$, $s = (4\pi/\lambda)\sin\theta$, λ is the wavelength and 2θ is the scattering angle]. Recent developments in experimental techniques (see *e.g.* Feigin & Svergun, 1987, ch. 8; Koch, 1991) allow one to register precise SAS curves over a wide range of scattering vectors and comprehensive data interpretation is therefore of great importance.

As solution scattering provides low-resolution structural information, it is usually interpreted in terms of homogeneous particles. Shape modeling is still one of the most frequently used approaches (Feigin & Svergun, 1987, ch. 3.5). The direct method of Stuhrmann (1970*b*) with the recent improvements of Svergun & Stuhrmann (1991) allows low-resolution shape determination using a straightforward procedure. As the scattering-length density of biopolymers in solution is by no means homogeneous, shape modeling or determination, in a strict sense, has to be applied to the 'shape scattering'

* On leave from the Institute of Crystallography, Russian Academy of Sciences, Leninsky prospekt 59, 117333 Moscow, Russia.

curves. The latter can be obtained by the contrast-variation technique (Stuhrmann & Kirste, 1965, 1967), where the excess scattering-length density of the particle is divided into two parts:

$$\rho(\mathbf{r}) = \overline{\rho}\rho_c(\mathbf{r}) + \rho_s(\mathbf{r}), \tag{1}$$

where $\rho_c(\mathbf{r}) = 1$ inside the particle and zero elsewhere, $\rho_s(\mathbf{r})$ describes the density fluctuations with respect to the average value $\overline{\rho} = \langle\rho(\mathbf{r})\rangle - \rho_0$ (ρ_0 is the solvent density). The SAS intensity from an ensemble of dissolved particles is then represented as a sum of three basic functions

$$I(s,\overline{\rho}) = \overline{\rho}^2 I_c(s) + \overline{\rho} I_{cs}(s) + I_s(s). \tag{2}$$

Here, $I_c(s)$ is the shape scattering curve, $I_s(s)$ is the scattering from inhomogeneities and $I_{cs}(s)$ is the cross term. By varying the scattering density of the solvent ρ_0, one obtains $I(s,\overline{\rho})$ at different contrasts $\overline{\rho}$, which makes it possible to evaluate the basic functions (if the scattering curves for three or more contrasts are available).

As seen from (2), contrast variation provides not only the shape scattering curve but also information about the inner structure of the particle. The latter is usually analyzed only in terms of the contrast behavior of the radius of gyration (Stuhrmann & Kirste, 1967). Only in special cases can a more detailed analysis be done, for example, for spherical particles (*e.g.* Cusack, Ruigrok, Krygsman & Mellema, 1985). In the present paper, new approaches to the evaluation of the internal structure of particles in solution are presented.

1. Multipole expansion

In this paper, we use extensively the formalism of the multipole expansion. The main equations are presented below but a more detailed description can be found in the original papers of Stuhrmann (1970*a*,*b*).

A particle density distribution $\rho(\mathbf{r})$ can be represented as a series

$$\rho(\mathbf{r}) \simeq \rho_L(\mathbf{r}) = \sum_{l=0}^{L}\sum_{m=-l}^{l} \rho_{lm}(r) Y_{lm}(\omega), \tag{3}$$

where $(r,\omega) = (r,\theta,\varphi)$ are spherical coordinates,

$$\rho_{lm}(r) = \int_\omega \rho(\mathbf{r}) Y^*_{lm}(\omega)\,\mathrm{d}\omega \tag{4}$$

are the radial functions and $Y_{lm}(\omega)$ are spherical harmonics. The truncation value L describes the resolution of the representation of the particle structure [$\rho_L(\mathbf{r}) \to \rho(\mathbf{r})$ when $L \to \infty$]. With this expansion, the particle SAS intensity is expressed as (Harrison, 1969; Stuhrmann, 1970*a*)

$$I(s) = 2\pi^2 \sum_{l=0}^{L}\sum_{m=-l}^{l} |A_{lm}(s)|^2. \tag{5}$$

Here, the partial amplitudes $A_{lm}(s)$ are given by the Hankel transforms of the radial functions

$$A_{lm}(s) = i^l (2/\pi)^{1/2} \int_0^\infty \rho_{lm}(r) j_l(sr) r^2\,\mathrm{d}r, \tag{6}$$

where $j_l(sr)$ are the spherical Bessel functions.

The aim of the SAS data interpretation using the multipole expansion is to distinguish between the different multipole contributions in $I(s)$, which would then allow restoration of the distribution $\rho(\mathbf{r})$. This is obviously impossible unless appropriate additional information about the particle structure is available, giving constraints on the $\rho(\mathbf{r})$ distribution [*e.g.* particle symmetry (Svergun, Feigin & Schedrin, 1982)]. One of the most important restrictions is the assumption that the particle is homogeneous. The structure of a wide variety of homogeneous particles can be described with the help of the angular shape function $F(\omega)$ as

$$\rho(\mathbf{r}) = \begin{cases} 1 & 0 \le r < F(\omega) \\ 0 & r \ge F(\omega). \end{cases} \tag{7}$$

This function can also be developed into the series

$$F(\omega) \simeq F_L(\omega) = \sum_{l=0}^{L}\sum_{m=-l}^{l} f_{lm} Y_{lm}(\omega), \tag{8}$$

where the multipole coefficients are complex numbers

$$f_{lm} = \int_\omega F(\omega) Y^*_{lm}(\omega)\,\mathrm{d}\omega.$$

The set of f_{lm} coefficients describes the shape of the particle at the given resolution. Representing the spherical Bessel function as a power series

$$j_l(sr) = \sum_{p=0}^{p_{\max}} d_{lp} (sr)^{l+2p}, \tag{9}$$

where

$$d_{lp} = (-1)^p / 2^p p! [2(l+p)+1]!!,$$

and substituting this series into (6), one obtains (Stuhrmann, 1970*b*)

$$\begin{aligned} A_{lm}(s) &= i^l (2/\pi)^{1/2} \sum_{p=0}^{p_{\max}} d_{lp} s^{l+2p} \int_\omega Y^*_{lm}(\omega)\,\mathrm{d}\omega \\ &\quad \times \int_{r=0}^{F(\omega)} r^{l+2p+2}\,\mathrm{d}r \\ &= (is)^l (2/\pi)^{1/2} \sum_{p=0}^{p_{\max}} [d_{lp} f_{lm}^{(l+2p+3)} / (l+2p+3)] s^{2p}, \end{aligned} \tag{10}$$

where

$$f_{lm}^{(q)} = \int_\omega [F(\omega)]^q Y^*_{lm}(\omega)\,\mathrm{d}\omega. \tag{11}$$

The coefficients of the power series of the partial amplitudes and hence the SAS intensity are thus expressed as a nonlinear combination of the multipole coefficients $f_{lm}^{(q)}$ of the shape function. These relationships can be used to find the shape by minimizing the deviations between the experimental and calculated intensity curves. With the improvements described by Svergun & Stuhrmann (1991), the method was shown to be useful for the shape determination up to the resolution of $L \simeq 7$, that is, for a rather detailed shape description (see *e.g.* König, Svergun, Koch, Hübner & Schellenberger, 1993).

2. Scattering from an inhomogeneous particle

Let us consider the general case of the inhomogeneous particle with the envelope described by the shape function $F(\omega)$. The particle density can be represented as

$$\rho(\mathbf{r}) = \begin{cases} \sum_{\nu=0}^{L} \sum_{\mu=-\nu}^{\nu} \rho_{\nu\mu}(r) Y_{\nu\mu}(\omega) & r \le F(\omega) \\ 0 & r > F(\omega), \end{cases} \tag{12}$$

with the radial functions $\rho_{\nu\mu}(r)$ expressed in terms of the power series

$$\rho_{\nu\mu}(r) = \sum_{n=0}^{N} c_{\nu\mu}^{(n)} r^n, \tag{13}$$

where the $c_{\nu\mu}^{(n)}$ are complex numbers. Substituting (12)–(13) into (6), one obtains for the partial amplitudes

$$\begin{aligned} B_{lm}(s) = i^l (2/\pi)^{1/2} & \sum_{p=0}^{p_{\max}} d_{lp} s^{l+2p} \\ & \times \sum_{\nu=0}^{L} \sum_{\mu=-\nu}^{\nu} \int_{\omega} Y_{\nu\mu}(\omega) Y_{lm}^*(\omega)\, \mathrm{d}\omega \\ & \times \sum_{n=0}^{N} c_{\nu\mu}^{(n)} \int_{r=0}^{F(\omega)} r^{l+n+2p+2}\, \mathrm{d}r. \end{aligned} \tag{14}$$

The integral over r again results in the power of the shape function $F(\omega)$ as in (10). In order to take the integral over ω, we make use of the expression for the product of two spherical harmonics (Edmonds, 1957, p. 63):

$$\begin{aligned} Y_{\nu\mu}(\omega) Y_{lm}^*(\omega) & \\ = (-1)^m \sum_{k=|l-\nu|}^{l+\nu} & \left[\frac{(2l+1)(2\nu+1)(2k+1)}{4\pi}\right]^{1/2} \\ \times & \begin{pmatrix} l & \nu & k \\ 0 & 0 & 0 \end{pmatrix} \begin{pmatrix} l & \nu & k \\ -m & \mu & m-\mu \end{pmatrix} Y_{\nu,m-\mu}^*(\omega), \end{aligned} \tag{15}$$

where $\begin{pmatrix} l & \nu & k \\ m & \mu & t \end{pmatrix}$ are $3j$ Wigner coefficients [equal to zero except for $t = -m-\mu$ (Edmonds, 1957, p. 45)].

Inserting (15) in (14), one obtains

$$\begin{aligned} B_{lm}(s) = (-1)^m (is)^l (2/\pi)^{1/2} & \\ \times \sum_{p=0}^{p_{\max}} d_{lp} s^{2p} & \sum_{\nu=0}^{L} \sum_{\mu=-\nu}^{\nu} \sum_{n=0}^{N} c_{\nu\mu}^{(n)} \\ \times \sum_{k=|l-\nu|}^{1+\nu} & \left[\frac{(2l+1)(2\nu+1)(2k+1)}{4\pi}\right]^{1/2} \\ \times & \begin{pmatrix} l & \nu & k \\ 0 & 0 & 0 \end{pmatrix} \begin{pmatrix} l & \nu & k \\ -m & \mu & m-\mu \end{pmatrix} \frac{f_{k,m-\mu}^{(l+n+2p+3)}}{l+n+2p+3}. \end{aligned} \tag{16}$$

This general expression enables one to evaluate the partial amplitudes for an inhomogeneous particle. They depend both on the coefficients $f_{lm}^{(q)}$ defining the particle shape and on the coefficients $c_{\nu\mu}^{(n)}$ describing the density distribution inside the particle. The scattering intensity of the particle is readily calculated from the partial amplitudes using (5). This expression therefore gives a convenient parameterization for the determination of the particle structure in the general case, in particular using contrast-variation data.

With a set of experimental data $\{I_e(s,\bar{\rho})\}$ for different contrasts, shape determination and evaluation of the inner structure can be done in two successive steps. Indeed, the shape scattering curve $I_c(s)$ can be evaluated first and the particle shape (*i.e.* the set of coefficients f_{lm}) can be determined following the procedure described by Svergun & Stuhrmann (1991). The representation (12)–(13) is then used to describe the density distribution of the inhomogeneities $\rho_s(\mathbf{r})$. As the shape coefficients $f_{lm}^{(q)}$ are already known, the partial amplitudes $B_{lm}(s)$ will depend only on $c_{\nu\mu}^{(n)}$. The same will be true for the scattering intensity at the contrast $\bar{\rho}$:

$$\begin{aligned} I_t(s,\bar{\rho}) &= I_t(s,\bar{\rho},\{c_{\nu\mu}^{(n)}\}) \\ &= 2\pi^2 \sum_{l=0}^{L} \sum_{m=-l}^{l} [\bar{\rho}^2 |A_{lm}(s)|^2 \\ &\quad + \bar{\rho} |A_{lm}(s) B_{lm}^*(s) + A_{lm}^*(s) B_{lm}(s)| + |B_{lm}(s)|^2] \end{aligned} \tag{17}$$

[here the amplitudes $A_{lm}(s)$ refer to the shape scattering and are evaluated according to (10)]. The coefficients $c_{\nu\mu}^{(n)}$ can then be found by minimizing the deviations between the set of experimental curves $\{I_e(s,\bar{\rho})\}$ and the theoretically evaluated curves (17), *e.g.* by minimizing

$$R_\rho = \frac{\sum_j \left(\int_{s_{\min}}^{s_{\max}} \{[I_e(s,\bar{\rho}_j) - I_t(s,\bar{\rho}_j)]/\sigma(s,\bar{\rho}_j)\}^2\, \mathrm{d}s \right)}{\sum_j \left\{ \int_{s_{\min}}^{s_{\max}} [I_t(s,\bar{\rho}_j)/\sigma(s,\bar{\rho}_j)]^2\, \mathrm{d}s \right\}}, \tag{18}$$

where the index j runs over the contrasts and the function $\sigma(s,\overline{\rho}_j)$ gives the experimental errors in the jth data set $I_e(s,\overline{\rho}_j)$. The function R_ρ is nonlinear with respect to the coefficients $c_{\nu\mu}^{(n)}$, therefore, its minimization requires optimization techniques similar to those used in the shape determination (Svergun & Stuhrmann, 1991).

The number of terms $N+1$ in the power series (13) representing the radial functions can be chosen as follows. It is natural to demand the same spatial resolution for the radial functions as for the envelope function. At a given radius R_0, the spatial resolution of the shape function provided by the series (7) is about $R_0\pi/L$. Since a polynomial of the $(N+1)$th degree can have at most $N+1$ zeros on $[0, R_0]$, the resolution of the radial function is approximately R_0/N, leading to the estimate $N \simeq L/\pi$.

The coefficients describing the shape and the radial functions of the inhomogeneities are not independent. Thus, by definition of $\rho_s(\mathbf{r})$,

$$\begin{aligned}\int_{F(\omega)} \rho_s(\mathbf{r})\,\mathrm{d}^3\mathbf{r} &= \sum_{\nu=0}^{L}\sum_{\mu=-\nu}^{\nu}\int_\omega Y_{\nu\mu}(\omega)\,\mathrm{d}\omega \sum_{n=0}^{N} c_{\nu\mu}^{(n)} \int_{r=0}^{F(\omega)} r^{n+2}\,\mathrm{d}r \\ &= \sum_{\nu=0}^{L}\sum_{\mu=-\nu}^{\nu}(-1)^\mu \sum_{n=0}^{N} c_{\nu\mu}^{(n)}[f_{\nu\mu}^{(n+3)}]^*/(n+3) = 0.\end{aligned} \tag{19}$$

Additional correlations can be obtained for the contrast dependence of the radius of gyration,

$$R_g^2(\overline{\rho}) = R_c^2 + \alpha/\overline{\rho} - \beta/\overline{\rho}^2 \tag{20}$$

[Stuhrmann & Kirste (1967); here, α and β are commonly accepted notations that should not be confused with the Euler angles used below]. The radius of gyration at infinite contrast obviously depends only on the shape coefficients ($R_c^2 = 3f_{00}^{(5)}/5f_{00}^{(3)}$), whereas for α one obtains

$$\begin{aligned}\alpha &= V_c^{-1}\int_{F(\omega)} \rho_s(\mathbf{r}) r^2\,\mathrm{d}^3\mathbf{r} \\ &= V_c^{-1}\sum_{\nu=0}^{L}\sum_{\mu=-\nu}^{\nu}(-1)^\mu \sum_{n=0}^{N} c_{\nu\mu}^{(n)}[f_{\nu\mu}^{(n+5)}]^*/(n+5),\end{aligned} \tag{21}$$

where $V_c = (4\pi/9)^{1/2} f_{00}^{(3)}$ is the particle volume. The equation for β involves coefficients $f_{\nu\mu}^{(n+4)}$ and is more complicated. These correlations can be used as additional constraints in the minimization of the function (18).

3. Scattering from fluctuations

The above formalism can be applied to a practically important case of scattering from density fluctuations, *i.e.* the inhomogeneities that are small in size compared to the particle itself. In many applications, *e.g.* when proteins of high molecular weight are studied, the particle is 'almost' homogeneous at the resolution normally achieved in SAS (about 3–4 nm; the shape scattering dominates in the corresponding range of momentum transfers). Even in such cases, however, the outer part of the scattering curve still contains a non-negligible contribution from the fluctuations that influence the results if one uses the homogeneous approximation without performing contrast variation. The following question is therefore of practical importance: given the particle shape, is it possible to estimate deviations from the shape scattering resulting from the high-frequency (*e.g.* for proteins of size about 1 nm) density fluctuations inside the particle?

Let us first consider a practical example that illustrates the influence and appearance of the intraparticle density fluctuations. In Fig. 1, the structure of formate dehydrogenase (molecular weight 86 kDa; Lamzin *et al.*, 1992) is shown at the different resolution levels: the trace of the C^α atoms is presented in Fig. 1(*a*) and the envelope function in Fig. 1(*b*) (the latter is evaluated from the atomic coordinates using harmonics up to $L = 7$ by the procedure briefly described in § 5). In Fig. 2(*a*), curve (1) corresponds to the shape scattering from the envelope function

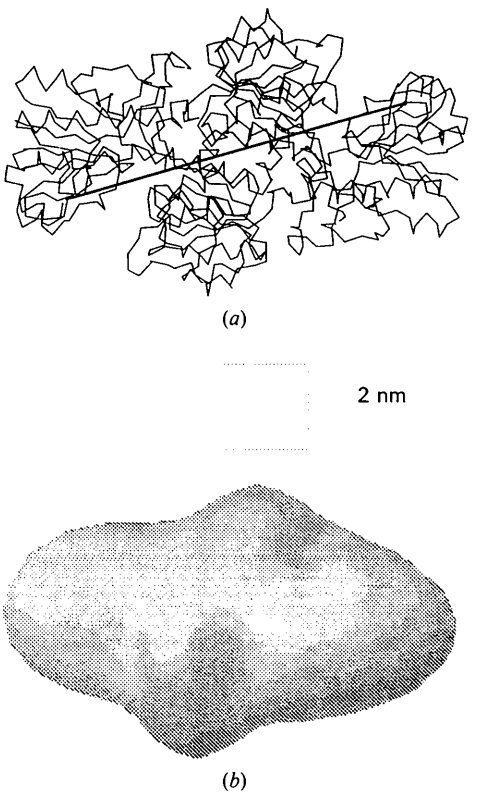

Fig. 1. Formate dehydrogenase (apo form): (*a*) C^α trace, (*b*) envelope function up to resolution $L = 7$.

whereas curve (2) is obtained from solution-scattering experiments. The two curves coincide well up to $s \simeq 1.5\ \text{nm}^{-1}$ but at higher momentum transfers the experimental curve goes systematically higher owing to the internal density fluctuations. Fig. 3 presents the particle density along the line shown in Fig. 1(*a*) evaluated from the electron-density map at 0.6 nm resolution, which gives a typical pattern of the density fluctuations inside the particle.

A general model of such fluctuations can be introduced in the following way. Let us assume that there are density fluctuations of magnitude 2Λ and size $\delta r << R_0$ inside a particle with a shape $F(\omega)$ and a characteristic size R_0. With no loss of generality, the density of fluctuations $\Delta\rho_f(\mathbf{r})$ can be represented as a product of its radial and angular components: $\Delta\rho_f(\mathbf{r}) = 2\Lambda\rho_f(r)g(\omega)$, where both components display the density fluctuations of average size δr. These conditions can be met by choosing

$$\begin{aligned}\Delta\rho_f(\mathbf{r}) &= \Delta\rho_f(\mathbf{r},\nu)\\ &= 2\Lambda\Delta\rho_f(r)\mathrm{Re}\,[Y_{\nu\mu}(\omega)]\\ &= \Lambda\Delta\rho_f(r)[Y_{\nu\mu}(\omega) + Y^*_{\nu\mu}(\omega)]\end{aligned} \tag{22}$$

inside the particle and $\Delta\rho_f(\mathbf{r}) = 0$ elsewhere. Here, the radial distribution of fluctuations $\Delta\rho(r)$ is a multistep function

$$\Delta\rho_f(r) = (-1)^{\mathrm{int}(r/\delta r)} \tag{23}$$

(Fig. 4*a*), whereas the order of harmonics ν should be taken in such a way that the average tangential fluctuation, $(\pi/\nu)R_0$, is equal to δr (Fig. 4*b*). The characteristic particle size (namely mean-squared size) is just the radius of gyration of its shape R_c, therefore,

$$\nu \simeq \pi R_c/\delta r. \tag{24}$$

Both radial and angular components vary in the range $[-1,1]$ and their product results in a three-dimensional oscillating density distribution inside the particle.

Inserting (22) into (6) and using again the power series expansion (9), one obtains for the partial amplitudes

$$\begin{aligned}B_{lm}(s) = 2\Lambda i^l(2/\pi)^{1/2} &\sum_{p=0}^{\infty} d_{lp}s^{l+2p}\\ &\times \int_{\omega} Y_{\nu\mu}(\omega)Y^*_{lm}(\omega)\,\mathrm{d}\omega\\ &\times \int_{r=0}^{F(\omega)} \Delta\rho_f(r)r^{l+2p+2}\,\mathrm{d}r\end{aligned} \tag{25}$$

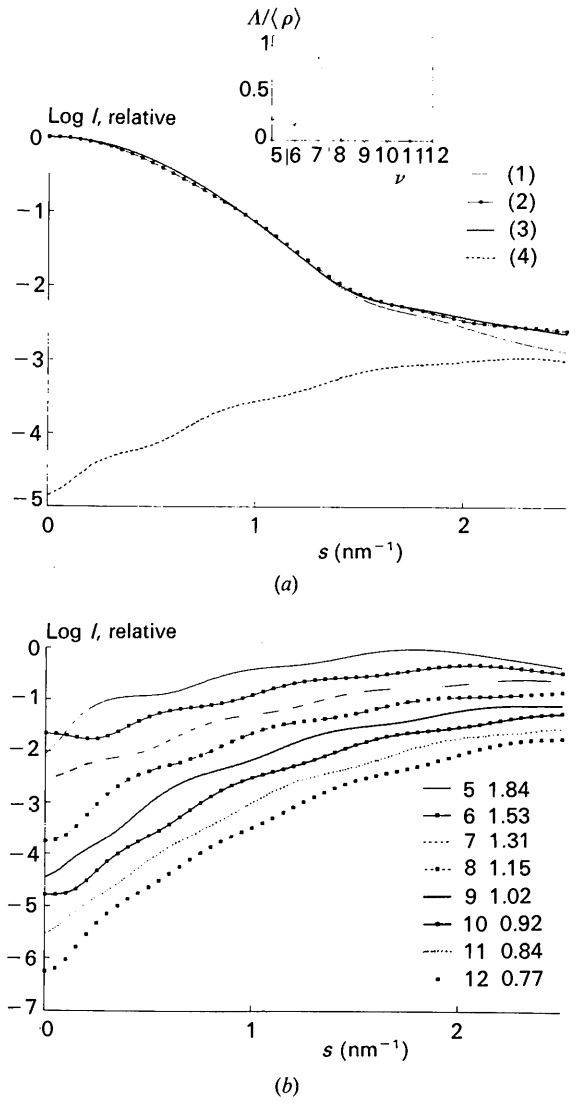

Fig. 2. Scattering from formate dehydrogenase. (*a*) (1) Shape scattering from the envelope function, (2) scattering in solution, processed experimental curve, (3) its fit using scattering from fluctuations, (4) net scattering from inhomogeneities. The weights Λ_ν are shown in the insert. (*b*) Scattering from fluctuations of different sizes (the orders of harmonics and the corresponding δr values are given in the list).

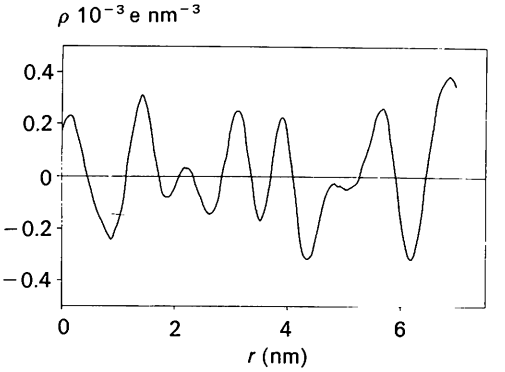

Fig. 3. Electron density in formate dehydrogenase along the line shown in Fig. 1(*a*). The zero level corresponds to a density of 250 e nm^{-3} (average electron density of the crystallographically ordered structure).

(for simplicity, we omit the complex conjugate of $Y_{\nu\mu}$; it is shown below that this makes no difference). The inner integral over r for the multistep function (23) is equal to $\delta r[F(\omega)]^{l+2p+2}/2$ (see Appendix). Again, using (15), one obtains

$$B_{lm}(s) = (-1)^m i^l (2/\pi)^{1/2} (\Lambda \delta r) \sum_{p=0}^{p_{\max}} d_{lp} s^{l+2p} \times \sum_{k=|l-\nu|}^{l+\nu} \left[\frac{(2l+1)(2\nu+1)(2k+1)}{4\pi}\right]^{1/2} \times \begin{pmatrix} l & \nu & k \\ 0 & 0 & 0 \end{pmatrix} \begin{pmatrix} l & \nu & k \\ -m & \mu & m-\mu \end{pmatrix} f^{(l+2p+2)}_{\nu, m-\mu}. \tag{26}$$

In fact, (22) describes a regularly, not statistically, distributed density of fluctuations. Hence, (26) does not yet adequately describe scattering from fluctuations: the partial amplitudes (and, therefore, the intensity) depend on the relative orientation of $F(\omega)$ and $Y_{\nu\mu}(\omega)$. This can be avoided by averaging the scattering intensity from fluctuations over these orientations. The relative orientation of $F(\omega)$ and $Y_{\nu\mu}(\omega)$ is changed when either of them is rotated [we describe the rotation by the Euler angles α, β, γ as defined by Edmonds (1957, p. 7)]. The results are more easily analyzed in terms of a rotating particle, the shape coefficients of which change owing to the rotations as

$$g^{(q)}_{lm}(\alpha\beta\gamma) = \prod_{\alpha\beta\gamma}\{f^{(q)}_{lm}\} = \sum_{m'=-l}^{l} \mathscr{D}^{(l)*}_{m'm}(\alpha\beta\gamma) f^{(q)}_{lm'}, \tag{27}$$

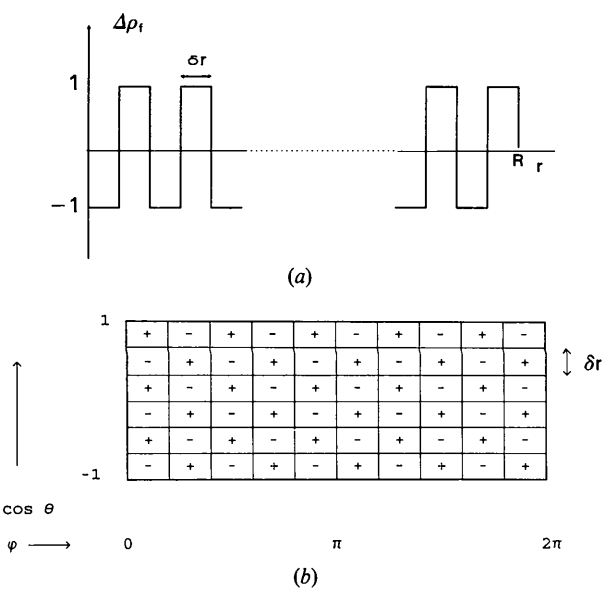

Fig. 4. (*a*) Radial and (*b*) angular components of the fluctuations [in (*b*), isolines $Y_{94}(\omega)=0$ are shown].

where $\mathscr{D}^{(l)}_{m'm}(\alpha\beta\gamma)$ is the operator of finite rotations [Edmonds (1957, p. 55); here, $(\alpha\beta\gamma)$ means dependence rather than product]. Note that the shape coefficients of all degrees change simultaneously according to (27) with the same operator $\mathscr{D}^{(l)}_{m'm}(\alpha\beta\gamma)$. The orthogonality of $\mathscr{D}^{(l)}_{m'm}(\alpha\beta\gamma)$ reads

$$(1/8\pi^2)\int_{\omega} \mathscr{D}^{(l_1)}_{m_1'm_1}(\alpha\beta\gamma)\mathscr{D}^{(l_2)*}_{m_2'm_2}(\alpha\beta\gamma)\,\mathrm{d}(\alpha\beta\gamma) = \delta_{m_1m_2}\delta_{m_1'm_2'}\delta_{l_1l_2}[1/(2l_1+1)], \tag{28}$$

where the integral is taken over all orientations and δ_{ij} is the Kronecker delta (equal to zero unless $i=j$). From these orthogonal properties, several important consequences can be deduced.

(i) The average value of each coefficient $g^{(q)}_{lm}$ is given by

$$\langle g^{(q)}_{lm}\rangle = \sum_{m'=-l}^{l} f^{(q)}_{lm'} \int_{\omega} \mathscr{D}^{(l)}_{m'm}(\alpha\beta\gamma)\,\mathrm{d}(\alpha\beta\gamma) = 0 \tag{29}$$

unless $l=m=0$. This means that the averaged scattering amplitude of the inhomogeneities is zero (the monopole term in the scattering from fluctuations has to be zero by definition). The same is true for the cross term between the shape scattering and the scattering from the fluctuations, which contains the averages of the cross products of the shape coefficients for the fixed and rotating particle, $\langle f^{(q_1)}_{l_1m_1} g^{(q_2)*}_{l_2m_2}\rangle = f^{(q_1)}_{l_1m_1}\langle g^{(q_2)*}_{l_2m_2}\rangle = 0$.

(ii) The average of the cross product $g^{(q_1)}_{l_1m_1} g^{(q_2)*}_{l_2m_2}$, where both coefficients belong to the rotating particle, is

$$\langle g^{(q_1)}_{l_1m_1} g^{(q_2)*}_{l_2m_2}\rangle = \delta_{m_1m_2}\delta_{m_1'm_2'}\delta_{l_1l_2}[1/(2l_1+1)] \times \sum_{m=-l_1}^{l_1} f^{(q_1)}_{l_1m} f^{(q_2)*}_{l_1m} = C(l_1,q_1,q_2). \tag{30}$$

This means that the cross terms between the coefficients with different indices (not different degrees!) will vanish in the scattering intensity from inhomogeneities.

(iii) As all the average cross products (30) depend only on the index l, the scattering intensity from inhomogeneities will not depend on the actual value of the index μ. This is what one could have expected given the fact that the order of integral transform (6) for the partial amplitudes depends only on l, not on m.

Using (29)–(30) and taking $\mu=0$ for simplicity [that is, $\Delta\rho_f(\mathbf{r},\nu) = 2\Lambda\Delta\rho_f(r)Y_{\nu 0}(\omega)$], one arrives at the following expression for the partial scattering intensities from the fluctuations of magnitude 2Λ and average size $\delta r \simeq \pi R_c/\nu$:

$$I_{lm}(s) = \langle B_{lm}(s)B^*_{lm}(s)\rangle = s^{2l}(\Lambda\delta r/\pi)^2(2l+1)(2\nu+1)/2$$

$$\times \sum_{p=0}^{2p_{max}} s^{2p} \sum_{t=\max(0,p-p_{max})}^{\min(p,p_{max})} d_{lt} d_{l,p-t}$$

$$\times \sum_{k=|l-\nu|}^{l+\nu} (2k+1) \begin{pmatrix} l & \nu & k \\ 0 & 0 & 0 \end{pmatrix}^2 \begin{pmatrix} l & \nu & k \\ -m & 0 & m \end{pmatrix}^2$$

$$\times C[k, l+2t+2, l+2(p-t)+2]. \quad (31)$$

The total scattering intensity $I_s(s)$ is again evaluated by summing up the multipole contributions according to (5).

The most important feature of the scattering from fluctuations as introduced here is that the cross term between the fluctuations and the shape scattering vanishes and the fluctuations term is additive. This means that the fluctuations do not correlate with the particle shape, although they are defined inside the particle, and therefore proves their 'quasistatistical' nature. In particular, the parameter α in equation (20) for R_g is always zero, which is what one should expect as the 'denser' and 'less dense' regions are uniformly distributed inside the particle.

In practice, the fluctuations do not have a fixed size and their density can be described as a linear superposition of the functions (22):

$$\Delta\rho_f(\mathbf{r}) = \sum_{\nu} \Lambda_\nu \Delta\rho_f(\mathbf{r}, \nu), \quad (32)$$

where the weight Λ_ν represents the magnitude of the fluctuation component of size $\delta r = \pi R_c / \nu$.

To illustrate the proposed approach, let us consider again the case of formate dehydrogenase. Fig. 2(*b*) presents the scattering evaluated from the fluctuation components with δr from 1.8 to 0.8 nm (corresponding to ν from 5 to 12). The experimental scattering curve can be well fitted using the shape scattering curve and the linear superposition (32) of these functions [curve (3) in Fig. 2*a*]. The amplitudes of fluctuations Λ_ν were allowed to range from zero up to the level of the average particle density $\langle\rho\rangle$; normalized amplitudes of the best fit $\Lambda_\nu/\langle\rho\rangle$ are presented in the insert in Fig. 2(*a*). The net scattering from fluctuations [curve (4) in Fig. 2*a*] corresponds to the average size of around 1.4 nm, in agreement with the profile presented in Fig. 3. Note that the amplitudes of the shorter fluctuation components are nearly zero in the fit because the information about smaller inhomogeneities is not contained in the range of momentum transfers used.

Another example is given by the myoglobin molecule, for which the influence of the inhomogeneities should be much stronger owing to its low molecular weight (17 kDa). The atomic coordinates of myoglobin (Watson, 1969) were taken from the Protein Data Bank (Bernstein *et al.*, 1977). In Fig. 5(*a*), the trace of the C^α atoms is shown. Fig. 5(*b*) presents the envelope function (resolution $L = 7$). In Fig. 6(*b*), the scattering from fluctuations with δr from 1 to 0.4 nm (ν from 5 to 12) is presented. Fig. 6(*a*) shows the shape scattering from the envelope in Fig. 5(*b*) [curve (1)] and the scattering intensity *in vacuo* evaluated from the atomic coordinates using the Debye formula [curve (2)] as well as its best fit using the superposition of fluctuations [curve (3); the normalized amplitudes $\Lambda_\nu/\langle\rho\rangle$ are shown in the insert]. In fact, such a small protein ($R_c = 1.5$ nm) already presents the limiting case for application of the concept of the scattering from fluctuations as its dimensions are comparable to the size of fluctuations. Thus, no good fit can be expected in the range $2 < s < 4\ \text{nm}^{-1}$ where the cross term plays a significant role. Nevertheless, for $s > 5\ \text{nm}^{-1}$, where the scattering from the inner structure dominates both the shape scattering and the cross term, the fit is much better and the net scattering from fluctuations [curve (4)] is in good agreement with the experimental data of Ibel & Stuhrmann (1975).

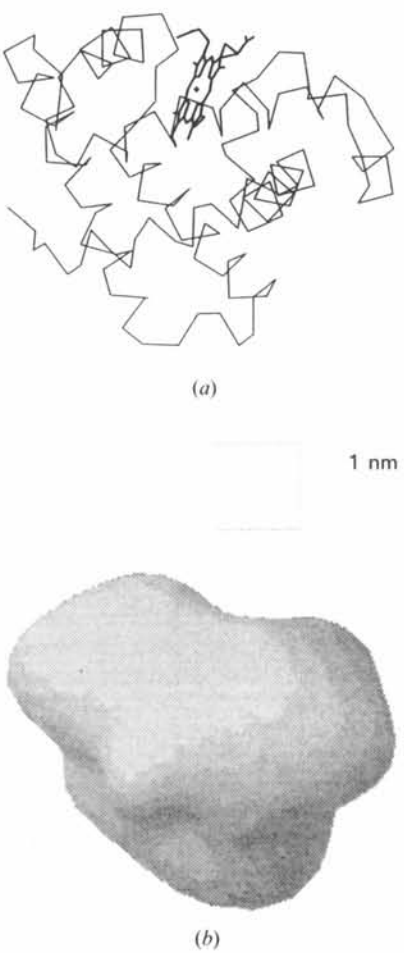

(*a*) (*b*)

Fig. 5. Myoglobin molecule: (*a*) C^α trace, (*b*) envelope function up to resolution $L = 7$.

4. Complex particles

Particles consisting of two or more components are of particular interest for contrast-variation studies as the additional information provided by contrast variation is represented in a very clear form. Let the particle have two distinct components A and B. The total scattering intensity is then

$$I(s,\bar{\rho}) = I(s,\bar{\rho}_a,\bar{\rho}_b) = 2\pi^2 \sum_{l=0}^{L} \sum_{m=-l}^{l} [\bar{\rho}_a^2 |A_{lm}(s)|^2 + \bar{\rho}_a\bar{\rho}_b |A_{lm}(s) B_{lm}^*(s) + A_{lm}^*(s) B_{lm}(s)| + \bar{\rho}_b^2 |B_{lm}(s)|^2], \quad (33)$$

where $\bar{\rho}_a$ and $\bar{\rho}_b$ are the contrasts of the components and $A_{lm}(s)$ and $B_{lm}(s)$ are their partial amplitudes. Contrast variation therefore separates the information about the structure of the two components (contained in the squared terms) and their relative position (contained in the cross term).

Let us assume that we know the partial amplitudes of the two components $A_{lm}(s)$ and $B_{lm}(s)$. Then, the scattering intensity will depend only on the relative position of the components. With the first component fixed, the relative position is described by the rotation of the second component by the Euler angles α, β and γ, followed by a displacement along the vector $\mathbf{u} = (u,\omega_u)$. The new partial amplitudes of the second component can be analytically expressed as (Svergun, 1991)

$$B_{lm}^{(s)}(s) = 4\pi(-1)^m \sum_{p=0}^{L} i^p j_p(su) \sum_{q=-p}^{p} Y_{pq}^*(\omega_u) \times \sum_{k=|l-p|}^{l+p} \begin{pmatrix} l & p & k \\ 0 & 0 & 0 \end{pmatrix} \times \sum_{t=-k}^{k} \left[\frac{(2l+1)(2p+1)(2k+1)}{4\pi}\right]^{1/2} \times \begin{pmatrix} l & p & k \\ -m & q & m-q \end{pmatrix} \mathscr{D}_{m-q,t}^{(k)}(\alpha\beta\gamma) B_{kt}(s). \quad (34)$$

The scattering intensity at each contrast (33) is thus expressed in terms of six parameters, which can be evaluated by minimizing function (18), and this allows one to determine the mutual positions of the components.

If the partial amplitudes of the components are not known, they should also be involved in the minimization procedure. Two practically important cases can be distinguished. If A and B are separate domains as in Fig. 7(*a*), they can be described by shape functions $F(\omega)$ and $G(\omega)$, respectively; these are developed into the series (8) and the amplitudes are expressed *via* the corresponding shape coefficients. The core–shell case where the particle consists

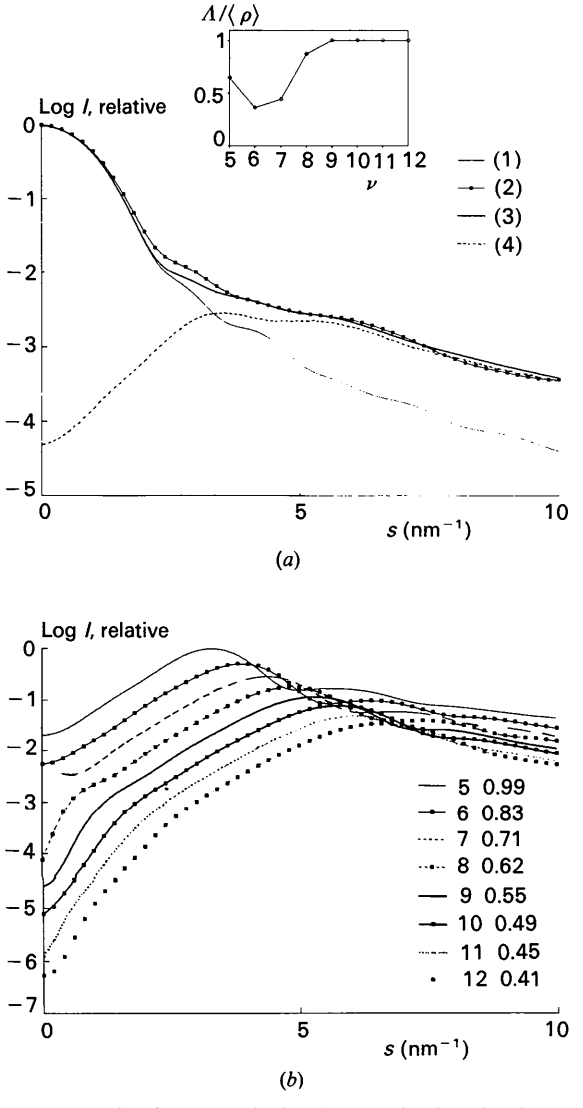

Fig. 6. Scattering from myoglobin. The notation is as in Figs. 2(*a*) and (*b*) except that curve (2) in (*a*) was evaluated from the atomic coordinates.

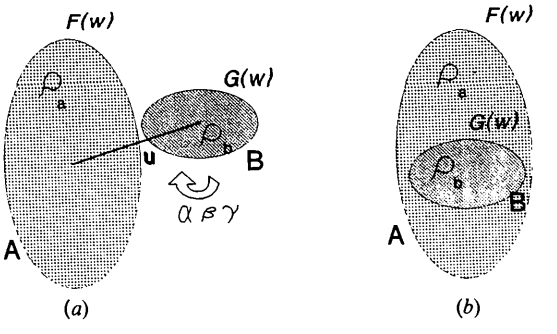

Fig. 7. Types of two-component particle: (*a*) two distinct domains; (*b*) core–shell model. For explanations see text.

of a compact core surrounded by a shell (Fig. 7*b*) is of particular practical importance. This situation is also described with the help of two shape functions: $F(\omega)$ corresponding to the whole particle and $G(\omega)$ corresponding to the core. Then, the two components entering (33) are defined as follows: component A is the particle of shape $F(\omega)$ and density $\rho_a = \rho_{\text{shell}}$ and component B is the particle of shape $G(\omega)$ and density $\rho_b = \rho_{\text{shell}} - \rho_{\text{core}}$.

For the two cases, the total intensity at each contrast (33) depends on the shape coefficients f_{lm} and g_{lm}, which are obtained by minimizing the function (18). The rotational and translational parameters are relevant only for the two-domain case. In the core–shell case, they are taken into account by the function $G(\omega)$ itself [its center of mass does not necessarily coincide with that of $F(\omega)$]. Note that, by definition of this model, $F(\omega) \geq G(\omega)$ for all ω, which means that the sets f_{lm} and g_{lm} cannot be independent of each other.

5. Program realization

The methods described above are implemented in a set of computer programs written in Fortran77 and tested on IBM-PC/MS-DOS, VAX/VMS and several Unix platforms (SPARC/Solaris, DEC/Ultrix, SGI/Irix). Together with the algorithms developed earlier for shape determination, they form a package containing more than 100 program entries.

An important additional tool included in the package is the generalized version of the indirect regularization program package *GNOM* (Svergun, Semenyuk & Feigin, 1988; Svergun, 1991, 1992). The program (called *CGNOM*) allows one reliably to decompose the experimental contrast-variation data

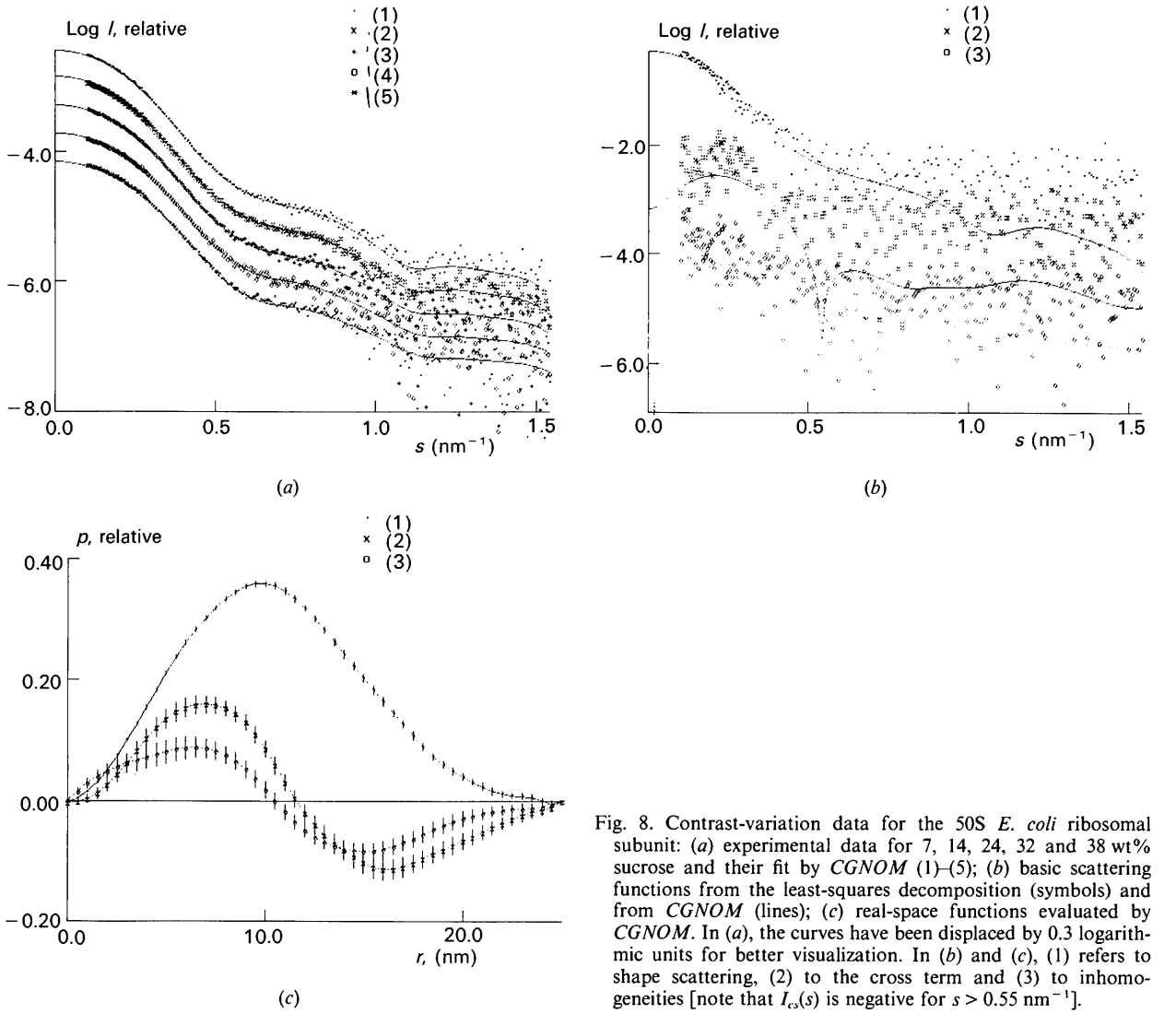

Fig. 8. Contrast-variation data for the 50S *E. coli* ribosomal subunit: (*a*) experimental data for 7, 14, 24, 32 and 38 wt% sucrose and their fit by *CGNOM* (1)–(5); (*b*) basic scattering functions from the least-squares decomposition (symbols) and from *CGNOM* (lines); (*c*) real-space functions evaluated by *CGNOM*. In (*a*), the curves have been displaced by 0.3 logarithmic units for better visualization. In (*b*) and (*c*), (1) refers to shape scattering, (2) to the cross term and (3) to inhomogeneities [note that $I_{cs}(s)$ is negative for $s > 0.55$ nm^{-1}].

into the basic scattering functions, the necessary first step in the use of the general approach [(12)–(18)]. The problem is less trivial than it may appear, especially in X-ray experiments where the range of contrasts is relatively narrow and the point-by-point solution of (2) with respect to the basic scattering functions can be unstable. This is illustrated in Fig. 8 for the data set obtained in the contrast-variation study of the 50S ribosomal subunit *E. coli* using synchrotron radiation (Svergun, Koch & Serdyuk, 1994). Five experimental curves presented in Fig. 8(*a*) were recorded at different sucrose contents ranging from 7 to 38 wt%. Their least-squares decomposition into (2) produces a result that can hardly be used for the further interpretation (Fig. 8*b*). The program *CGNOM* uses the regularization method to evaluate the generalized real-space distribution function

$$p(r,\overline{\rho}) = \overline{\rho}^2 p_c(r) + \overline{\rho} p_{cs}(r) + p_s(r), \qquad (35)$$

where each basic function in real space is connected by the Fourier transform to the corresponding basic scattering curve in (2). The experimental data at all contrasts are used simultaneously, which significantly improves the stability of the solution. The real-space functions evaluated from the data shown in Fig. 8(*a*) are presented in Fig. 8(*c*). Their Fourier transform yields the basic scattering curves presented in Fig. 8(*b*).

It is worth noting the several numerical peculiarities implemented in the algorithms described above. As the methods are to be used in the broad range of scattering vectors, precautions must be taken concerning the convergence of the power series of type (10). To improve the convergence, we use the so-called diagonal Padé approximant with the coefficients of the power series representation of a function $f(x)$ transformed into the rational approximation

$$f(x) = \sum_{k=0}^{2k_{max}} a_k x^k = \sum_{k=0}^{k_{max}} b_k x^k \Big/ \left(1 + \sum_{k=1}^{k_{max}} c_k x^k\right). \qquad (36)$$

The routine used to evaluate coefficients b_k and c_k from the given set of a_k is taken from Press, Teukolsky, Vetterling & Flannery (1992). Using the Padé approximant with $k_{max} = 20$ [that is, $p_{max} = 39$ in series (10)], scattering curves up to $sR_c \simeq 20$–25 can be evaluated.

To check quickly the conditions $F(\omega) \geq G(\omega) \geq 0$, a quasi-uniform angular grid on the surface of a sphere is generated using the following algorithm (G. Vriend, 1992, private communication):

$$\left.\begin{aligned} \theta_i &= \arccos[1 - 2(i-1)/f_k] \\ \varphi_i &= 2\pi \bmod [(i-1) + f_{k-1}, f_k]/f_k \end{aligned}\right\} \quad i = 1,..f_k + 1, \qquad (37)$$

where f_k is the kth Fibonacci number (defined as $f_k = f_{k-1} + f_{k-2}, f_0 = f_1 = 1$). The shape functions $F(\theta_i,\varphi_i)$ are evaluated on the grid for $\overline{k} = 11$ with $f_k + 1 = 145$ directions, which is sufficient to evaluate the integral measure of negativity

$$N(F) = \left[\int_{\omega^-} F(\omega)^2 \, d\omega \Big/ \int F(\omega)^2 \, d\omega\right]^{1/2}, \qquad (38)$$

where the first integral is taken over the negative $F(\omega)$ [$N(F) = 0$ if $F(\omega)$ is always positive]. The measures for the functions $F(\omega)$, $G(\omega)$ and $H(\omega) = F(\omega) - G(\omega)$ are added as penalties to the function (18). The Fibonacci grids with larger numbers of directions (*e.g.* $k = 14$, $f_k + 1 = 611$) are used to generate the three-dimensional models for graphic visualization (*cf.* Figs. 1*b* and 5*b*) and to evaluate the envelope functions of proteins from the atomic coordinates. In the latter case, the origin is selected in the center of mass of the protein and for each direction the most distant atom is found.

Instrumental effects leading to the smearing of the experimental data often play a significant role (Feigin & Svergun, 1987, ch. 9) and should therefore be taken into account. There are two ways to deal with the problem. One way is to desmear the experimental data, which can be done with the help of the program *CGNOM*. Another possibility is to smear the theoretical curves and minimize the function (18) in the 'smeared' reciprocal space. The instrumental smearing can be described with the help of the resolution function $R(s,s')$ as

$$J(s) = \int I(s') R(s,s') \, ds' \qquad (39)$$

[here, $J(s)$ is the smeared curve]. Pedersen, Posselt & Mortensen (1990) derived the expressions approximating $R(s,s')$ by a Gaussian function with the variable width depending on the instrumental setting and the actual value of the momentum transfer s. This approach is incorporated in the methods described above for fast smearing of the theoretical data. Direct fitting of the smeared experimental data is preferable when the range of contrasts is wide and the smearing effects are strong. This is the case in neutron scattering [for the spherically symmetric models such fitting was made, for example, by Cusack *et al.* (1985) and Pedersen (1993)].

6. Discussion

The methods described above are aimed at extracting more structural information from the SAS data than in the homogeneous particle approximation. A natural question that arises is whether this is justified given the restricted information content inherent in solution scattering, that is, whether the additional information contained in the contrast-variation experiments allows the more general representations of the particle structure to be used.

Let us consider the problem of the information content for the general approach [(12)–(18)]. From the Shannon sampling theorem, a scattering curve from a particle with maximum size D in the angular interval $[0,s_{max}]$ contains information about $K \simeq s_{max}D/\pi$ independent parameters (Moore, 1980; Taupin & Luzzati, 1982). There is at least one extra parameter, namely, the value of $I(0)$, which is often forgotten [Shannon sampling refers to the function $sI(s)$, thus $I(0)$ gets lost]. According to this estimate, a set of K_1 contrast-variation curves would provide $3K + K_1$ independent parameters (three basic scattering curves plus the forward-scattering values that can be evaluated independently for each curve). On the other hand, the number of unknowns to be found is $(L+1)^2$ [as $F(\omega)$ is real, one has $f_{l,-m} = (-1)^m f_{lm}$ and $\mathrm{Im}\,(f_{lm}) \equiv 0$ for $m = 0$]. Each degree in the power series of the radial functions (13) brings the same additional number of unknowns. The characteristic ratio is thus

$$R_N = \frac{\text{Number of unknowns}}{\text{Number of parameters}} = \frac{(N+2)(L+1)^2}{3K+K_1}. \tag{40}$$

With the linear approximation of the radial functions ($N=1$), this ratio is better than that of the shape determination [the latter is $(L+1)^2/(K+1)$]. Enhancement of the radial functions may worsen the ratio (depending on how many curves are available). Note, however, that (40) in fact gives an upper limit of R_N as the unknowns are not independent. Thus, the number of independent parameters is lowered by six, owing to the arbitrary orientation and the position of the center of mass (Svergun & Stuhrmann, 1991). Additional restrictions result from the positivity of $F(\omega)$, from the known shape invariants (volume, surface, radius of gyration), as well as from the correlations (19) and (21). The effective number of unknowns is significantly reduced when *a priori* information about the particle symmetry is available, which leads to the selection rules for the harmonics to be used (see *e.g.* König *et al.*, 1993).

For the other cases considered in this paper, the R_N ratio is more favorable. Thus, the fluctuations are described with the help of a few parameters (Λ_ν for higher harmonics). For the case of the two subparticles with known structures, one has the fixed number of six parameters. The core–shell model is described by $2(L+1)^2-6$ coefficients, which are, again, not independent. Note that the models shown in Fig. 6 do not include the inhomogeneities inside the single domain, which can be taken into account using the scattering from fluctuations (32)–(33).

The proposed approaches cover a wide range of possible practical applications. The method of (12)–(18) represents a new general algorithm for the joint analysis of the contrast-variation data and allows both shape and structure determinations. The search of the mutual positions of domains in complex particles can be effectively used to investigate the conformational changes in proteins with known crystallographic structure. The core–shell model adequately describes a wide variety of nucleoproteins and lipoproteins (ribosomal subunits, viruses, low-density lipoproteins *etc.*). The methods have been applied in the data interpretation of the contrast-variation experiments on the 50S ribosomal subunit of *E. coli* (Svergun, Koch & Serdyuk, 1994; Svergun, Koch, Pedersen & Serdyuk, 1994). The experimental data presented here in Fig. 8(*a*) also give a numerical example of estimation of the R_N ratio. The maximum size of the 50S subunit is 25 nm and the five scattering curves contain approximately $3 \times (25 \times 1.5)/\pi + 5 = 41$ parameters. At the resolution $L=5$, a core–shell model is described by $2 \times 6^2 - 6 = 66$ values, which gives $R_N = 1.6$. Bearing in mind that the unknowns are still correlated because of the conditions $F(\omega) \geq G(\omega) \geq 0$, one can therefore justify the use of harmonics up to $L=5$ in the core–shell model.

With the methods described in the analysis of the contrast-variation data, normal precautions should be taken concerning the solvent influence [*e.g.* inhomogeneous hydrogen exchange in neutron scattering (Witz, 1983)]. On the other hand, these methods are not restricted to classical contrast variation by solvent exchange. They can also be applied to the results of 'physical' contrast variation [*e.g.* by anomalous X-ray scattering (Stuhrmann, 1981) or spin-dependent neutron scattering (Stuhrmann, 1989)] provided the contrast dependencies derived for these particular cases are used.

The author is indebted to Dr M. Koch, Professor H. Stuhrmann and Dr J. Skov Pedersen for fruitful discussions and valuable comments on the manuscript. He thanks Dr J. Skov Pedersen for the smearing routines and Dr V. Lamzin for the experimental data on formate dehydrogenase. This work was supported by the NATO Linkage Grant LG 921231.

APPENDIX

To evaluate the integral

$$K(F,q) = \int_0^F \Delta\rho_f(r) r^q \,\mathrm{d}r, \tag{41}$$

where $\Delta\rho_f(r)$ is the multistep function (23), it can be rewritten as a sum of integrals

$$K(F,q) = \sum_{j=1}^{2M} (-1)^j \int_{(j-1)\delta r}^{j\delta r} r^q \,\mathrm{d}r$$

$$= [2(\delta r)^{q+1}/(q+1)]$$

$$\times\left[\sum_{j=1}^{2M}(-1)^j j^{q+1}-(2M)^{q+1}/2\right]$$

$$=[2(\delta r)^{q+1}/(q+1)]\left[\sum_{j=1}^{2M} j^{q+1}-2\right.$$

$$\left.\times\sum_{j=1}^{M}(2j-1)^{q+1}-(2M)^{q+1}/2\right], \quad (42)$$

where $2M$ is the number of steps (an even number, as seen in Fig. 4*a*). The two sums in square brackets can be expressed (Gradshtein & Ryzhik, 1963) as

$$\sum_{j=1}^{2M} j^{q+1}=(2M)^{q+2}/(q+2)+(2M)^{q+1}/2$$

$$+(q+1)(2M)^q/12+\ldots \quad (43)$$

$$\sum_{j=1}^{M}(2j-1)^{q+1}=(2M)^{q+2}/2(q+2)$$

$$-(q+1)(2M)^q/12+\ldots \quad (44)$$

(for $2M>>1$, its degrees of $q-1$ and less can be omitted). Substituting (43)–(44) into (42) and taking into account that $F=2M(\delta r)$, one obtains $K(F,q)\simeq \delta r\, F^q/2$.

References

BERNSTEIN, F. C., KOETZLE, T. F., WILLIAMS, G. J. B., MEYER, E. F. JR, BRICE, M. D., RODGERS, J. R., KENNARD, O., SHIMANOUCHI, T. & TASUMI, M. (1977). *J. Mol. Biol.* **112**, 535–542.

CUSACK, S., RUIGROK, R. W. H., KRYGSMAN, P. C. J. & MELLEMA, J. E. (1985). *J. Mol. Biol.* **186**, 565–582.

EDMONDS, A. R. (1957). *Angular Momentum in Quantum Mechanics*. Princeton, NJ: Princeton Univ. Press.

FEIGIN, L. A. & SVERGUN, D. I. (1987). *Structure Analysis by Small-Angle X-ray and Neutron Scattering*. New York: Plenum Press.

GRADSHTEIN, I. S. & RYZHIK, I. M. (1963). *Tablicy Integralow, Summ, Ryadow i Proizwedenij*, pp. 15–16. Moscow: Fizmatgiz. (In Russian.)

HARRISON, S. C. (1969). *J. Mol. Biol.* **42**, 457–483.

IBEL, K. & STUHRMANN, H. B. (1975). *J. Mol. Biol.* **93**, 255–265.

KOCH, M. H. J. (1991). *Handbook on Synchrotron Radiation*, edited by E. EBASHI, M. KOCH & E. RUBENSTEIN, pp. 241–268. Amsterdam: North Holland.

KÖNIG, S., SVERGUN, D. I., KOCH, M. H. J., HÜBNER, G. & SCHELLENBERGER, A. (1993). *Eur. Biophys. J.* **22**, 185–194.

LAMZIN, V. S., ALESHIN, A. E., STROKOPYTOV, B. V., YUKHNEVICH, M. G., POPOV, V. O., HARUTYUNYAN, E. H. & WILSON, K. S. (1992). *Eur. J. Biochem.* **206**, 441–452.

MOORE, P. B. (1980). *J. Appl. Cryst.* **13**, 168–175.

PEDERSEN, J. S. (1993). *Eur. Biophys. J.* **22**, 79–95.

PEDERSEN, J. S., POSSELT, D. & MORTENSEN, K. (1990). *J. Appl. Cryst.* **23**, 321–333.

PRESS, W. H., TEUKOLSKY, S. A., VETTERLING, W. T. & FLANNERY, B. P. (1992). *Numerical Recipes*, p. 192. Cambridge Univ. Press.

STUHRMANN, H. B. (1970*a*). *Acta Cryst.* A**26**, 297–306.

STUHRMANN, H. B. (1970*b*). *Z. Phys. Chem. (Frankfurt am Main)*, **72**, 177–184, 185–198.

STUHRMANN, H. B. (1981). *Q. Rev. Biophys.* **14**, 433–460.

STUHRMANN, H. B. (1989). *Physica (Utrecht)*, B**156&157**, 444–451.

STUHRMANN, H. B. & KIRSTE, R. G. (1965). *Z. Phys. Chem. (Frankfurt am Main)*, **46**, 247–250.

STUHRMANN, H. B. & KIRSTE, R. G. (1967). *Z. Phys. Chem. (Frankfurt am Main)*, **56**, 333–337.

SVERGUN, D. I. (1991). *J. Appl. Cryst.* **24**, 485–492.

SVERGUN, D. I. (1992). *J. Appl. Cryst.* **25**, 495–503.

SVERGUN, D. I., FEIGIN, L. A. & SCHEDRIN, B. M. (1982). *Acta Cryst.* A**38**, 827–835.

SVERGUN, D. I., KOCH, M. H. J., PEDERSEN, J. S. & SERDYUK, I. N. (1994). *J. Mol. Biol.* Submitted.

SVERGUN, D. I., KOCH, M. H. J. & SERDYUK, I. N. (1994). *J. Mol. Biol.* Submitted.

SVERGUN, D. I., SEMENYUK, A. V. & FEIGIN, L. A. (1988). *Acta Cryst.* A**44**, 244–250.

SVERGUN, D. I. & STUHRMANN, H. B. (1991). *Acta Cryst.* A**47**, 736–744.

TAUPIN, D. & LUZZATI, V. (1982). *J. Appl. Cryst.* **15**, 289–300.

WATSON, H. C. (1969). *Prog. Stereochem.* **4**, 299–333.

WITZ, Z. (1983). *Acta Cryst.* A**39**, 706–711.